NAVAL POSTGRADUATE SCHOOL

MONTEREY, CALIFORNIA

THESIS

ACOUSTIC NOISE INTERFEROMETRY

by

Rodney D. Thatcher

June 2020

Thesis Advisor: Oleg A. Godin
Second Reader: Kevin B. Smith

Approved for public release. Distribution is unlimited.

THIS PAGE INTENTIONALLY LEFT BLANK

REPORT DOCUMENTATION PAGE	*Form Approved OMB No. 0704-0188*

1. AGENCY USE ONLY *(Leave blank)*	**2. REPORT DATE** June 2020	**3. REPORT TYPE AND DATES COVERED** Master's thesis

4. TITLE AND SUBTITLE
ACOUSTIC NOISE INTERFEROMETRY

5. FUNDING NUMBERS

6. AUTHOR(S) Rodney D. Thatcher

7. PERFORMING ORGANIZATION NAME(S) AND ADDRESS(ES)
Naval Postgraduate School
Monterey, CA 93943-5000

8. PERFORMING ORGANIZATION REPORT NUMBER

9. SPONSORING / MONITORING AGENCY NAME(S) AND ADDRESS(ES)
National Science Foundation, Alexandria, VA 22314

10. SPONSORING / MONITORING AGENCY REPORT NUMBER

11. SUPPLEMENTARY NOTES The views expressed in this thesis are those of the author and do not reflect the official policy or position of the Department of Defense or the U.S. Government.

12a. DISTRIBUTION / AVAILABILITY STATEMENT
Approved for public release. Distribution is unlimited.

12b. DISTRIBUTION CODE
A

13. ABSTRACT (maximum 200 words)

Acoustic noise interferometry uses long time series recordings of ambient and shipping noise, which are concurrently captured at two locations, to measure the acoustic Green's function. With this technique, each hydrophone becomes a virtual acoustic transceiver—a combination of a source and a receiver—which can be used for passive acoustic remote sensing of the ocean. Compared to active techniques, passive remote sensing greatly reduces costs and allows for undetected, surreptitious monitoring of acoustic non-reciprocity, a sensitive measure of the velocity of oceanic currents. Using data obtained in the 2012 Florida Straits Noise Interferometry Experiment, this work investigated the feasibility of retrieval of the depth-dependence of the current velocity from the passively measured non-reciprocity of normal mode travel times in a shallow-water waveguide. It was found that measurements of the current-induced non-reciprocity of normal mode group speeds with errors up to 0.2 m/s will allow for inversion of the vertical current velocity profile with oceanographically relevant vertical resolution and accuracy. Additionally, passive measurements of acoustic non-reciprocity at frequencies below 80 Hz at ranges of about 50 times the ocean depth are sufficient for retrieval of the current velocity profile in shallow water. Thus, the technique investigated in the thesis can now be applied to field data, like those acquired in previous measurements in the Florida Straits.

14. SUBJECT TERMS noise interferometry, hydrophones, acoustics, passive remote sensing, reciprocity in acoustics	**15. NUMBER OF PAGES** 55
	16. PRICE CODE

17. SECURITY CLASSIFICATION OF REPORT	**18. SECURITY CLASSIFICATION OF THIS PAGE**	**19. SECURITY CLASSIFICATION OF ABSTRACT**	**20. LIMITATION OF ABSTRACT**
Unclassified	Unclassified	Unclassified	UU

NSN 7540-01-280-5500

Standard Form 298 (Rev. 2-89)
Prescribed by ANSI Std. 239-18

THIS PAGE INTENTIONALLY LEFT BLANK

Approved for public release. Distribution is unlimited.

ACOUSTIC NOISE INTERFEROMETRY

Rodney D. Thatcher
Lieutenant, United States Navy
BS, University of South Carolina, 2013

Submitted in partial fulfillment of the
requirements for the degree of

MASTER OF SCIENCE IN APPLIED PHYSICS

from the

NAVAL POSTGRADUATE SCHOOL
June 2020

Approved by: Oleg A. Godin
Advisor

Kevin B. Smith
Second Reader

Kevin B. Smith
Chair, Department of Physics

THIS PAGE INTENTIONALLY LEFT BLANK

ABSTRACT

Acoustic noise interferometry uses long time series recordings of ambient and shipping noise, which are concurrently captured at two locations, to measure the acoustic Green's function. With this technique, each hydrophone becomes a virtual acoustic transceiver—a combination of a source and a receiver—which can be used for passive acoustic remote sensing of the ocean. Compared to active techniques, passive remote sensing greatly reduces costs and allows for undetected, surreptitious monitoring of acoustic non-reciprocity, a sensitive measure of the velocity of oceanic currents. Using data obtained in the 2012 Florida Straits Noise Interferometry Experiment, this work investigated the feasibility of retrieval of the depth-dependence of the current velocity from the passively measured non-reciprocity of normal mode travel times in a shallow-water waveguide. It was found that measurements of the current-induced non-reciprocity of normal mode group speeds with errors up to 0.2 m/s will allow for inversion of the vertical current velocity profile with oceanographically relevant vertical resolution and accuracy. Additionally, passive measurements of acoustic non-reciprocity at frequencies below 80 Hz at ranges of about 50 times the ocean depth are sufficient for retrieval of the current velocity profile in shallow water. Thus, the technique investigated in the thesis can now be applied to field data, like those acquired in previous measurements in the Florida Straits.

THIS PAGE INTENTIONALLY LEFT BLANK

TABLE OF CONTENTS

THIS PAGE INTENTIONALLY LEFT BLANK

LIST OF FIGURES

LIST OF TABLES

THIS PAGE INTENTIONALLY LEFT BLANK

LIST OF ACRONYMS AND ABBREVIATIONS

AAV	amphibious assault vehicle
CCF	cross-correlation coefficient
ESSP	effective sound speed profile
GF	Green's Function
MIW	mine warfare
MSP	multi-scale profiler
NCCF	noise cross-correlation coefficient
RMSE	root mean square error
SSP	sound speed profile

THIS PAGE INTENTIONALLY LEFT BLANK

ACKNOWLEDGMENTS

I would like to share my deepest gratitude for the mentorship and intellectual support from my advisor, Dr. Oleg Godin, and Dr. Tsu Wei Tan in the development and writing of this thesis.

To my loving wife, thank you for your patience and support through the late nights and frustrations. I wouldn't have been able to accomplish this without your encouragement.

THIS PAGE INTENTIONALLY LEFT BLANK

I. INTRODUCTION

A. BACKGROUND

A wealth of information can be uncovered by analyzing ambient noise in the ocean. The underwater environment affects the propagation of sound in a variety of ways that can then be measured and used as a probe to characterize the conditions in the fluid medium and boundaries. These properties are of great interest to the U.S. Navy to develop an understanding of the bottom type, ocean currents, and noise levels for use in amphibious, mine hunting, and intelligence gathering operations.

Traditionally, these properties were gathered by use of active sources such as air guns or sonar in an overt manner. These methods are costly and require an exuberant amount of resources and manpower. In addition, they are also easily differentiable from the ambient noise, which could result in unwanted detection. Utilization of ambient noise from shipping, wind, rain, and marine life provides for surreptitious, cost effective, and continuous monitoring of conditions. It can then provide for clandestine operations with minimization of risk of discovery, manpower, and resources. Instead of needing to insert a survey team or platform to gather information about the shallow water environment, the currents and sea floor properties can be gathered covertly in support of planning operations for amphibious assault vehicles (AAV) and mine warfare (MIW). As an added benefit, this method also has minimal impact to the marine ecosystem. This is all possible due to passive acoustic noise interferometry.

B. NOISE INTERFEROMETRY

Acoustic noise interferometry, otherwise known as Green's function retrieval from ambient noise cross-correlation, allows for approximating the properties of the seabed and water column by means of ambient noise through a minimum of two spatially separated hydrophones. By cross-correlating the time series of diffuse ambient noise concurrently measured at two locations to retrieve the acoustic Green's function approximation, or impulse response, the two receivers can act as a virtual source and receiver pair. In the paper titled *Ocean Tomography with Acoustic Daylight* by Godin et al., diffuse ambient

noise is referred to as acoustic daylight; just as sunlight is used to observe and distinguish the surrounding environment, diffuse ambient noise can be used to view the ocean [1]. The noise cross-correlation function (NCCF) can be calculated as

$$C_{AB} = \frac{1}{T}\int_0^T p(x_A, t+\tau)\, p(x_B, t) dt\,. \tag{1}$$

Equation 1 is the NCCF measured at the points *A* and *B* and averaged over a length of time *T*. The measure of the acoustic field is given by *p* with respect to time *t* and time delay τ. The time delay is determined by the acoustic travel times between the two hydrophones. The method of use to retrieve the Green's function approximation is well discussed in [2], [3], and [4].

From the NCCF the Green's function approximation can be received to get deterministic data in order to create a virtual transceiver. The travel time between the virtual source and receiver can then be used to construct dispersion curves of normal modes to further probe the ocean [5].

C. RECIPROCAL TRANSMISSION

Given a source and receiver separated by an arbitrary distance, the travel time of the direct path ray will be the same even if the source and receiver positions are swapped, as discussed in chapter 2 of *Ocean Acoustic Tomography* [6]. The medium the pressure wave travels through does not need to be homogenous or lossless as the pressure wave will encounter the same losses from attenuation and boundaries traveling in either direction. Thus in the absence of flow the travel time between two points is reciprocal. This is commonly known as acoustic reciprocity.

In the event the medium is subject to currents the travel time in the opposite direction will not be equal, resulting in the breaking down of acoustic reciprocity. In the 2014 article by Godin et al. based on the 2012 Florida Straits Experiment, non-reciprocity of diffuse ambient and shipping noise in the shallow water waveguide of the Florida Straits was used to determine the depth-averaged current profile [7]. Three hydrophones placed 15 km off the Florida Keys at 100 meters depth were used in different pairs to observe the

shift in the waveform to get the depth-averaged velocity. Noticeable shifts in the waveform due to the strong Florida Straits currents were recorded, as seen in Figure 1.

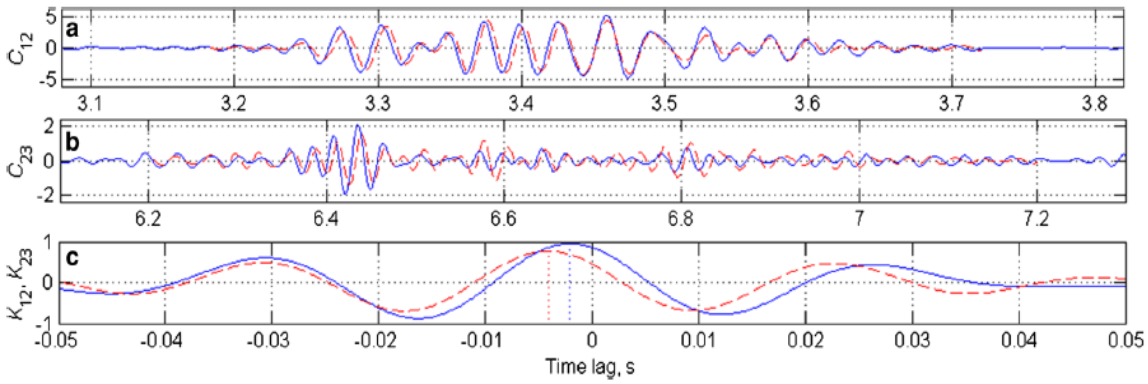

(a) NCCF C_{12} for receivers separated by 5 km is shown by the solid blue and dashed red lines for the positive and negative time delays respectively. (b) same as in (a) NCCF C_{23} for receivers separated by 9.6 km. (c) is correlation between +/- time delays.

Figure 1. Comparison of the structure of noise cross-correlations at positive and negative time delays. Adapted from [7].

The non-reciprocity in Figure 1 is manifested due to down-current travel time being shorter than up current. The time delay can then be used to determine the depth-averaged flow velocity without in depth knowledge of the noise sources, SSP, or bottom characteristics. As this method finds only the depth-averaged flow velocity, this thesis investigates the possibility of creating a depth dependent profile by extending this concept to the separation of normal modes.

D. GOALS OF RESEARCH

Previous work by Godin et al. [7] and Brown et al. [8] discussed using the data gathered in the 2012 Florida Straits noise interferometry experiment to determine the depth-averaged current velocity from the current induced time delay. Using the same data, Tan et al. followed with focusing on characterizing the sea floor off of reciprocal (mean of travel times) component of the group speed which, discussed but not investigated, can also be used to find the depth-dependent current velocity profile [5]. As continuation of that

work, this thesis intends to investigate the ability to determine the depth-dependent velocity profile and characterize the necessary accuracy of measurement of the modal group speed.

II. METHODS

A. EFFECTIVE SOUND SPEED APPROXIMATION

The effective sound speed profile (ESSP) is in essence the substitution of a motionless effective sound speed in place of the sound speed in a moving fluid. As discussed in Dr. Godin's 2002 article in *Acoustical Society of America*, this idea of simplifying the moving fluid with a motionless one was first introduced by Lord Rayleigh [9]. Essentially, the current velocity effect on the acoustic field is approximately equivalent to the projection of current velocity, from source to receiver, on the SSP. When the direction of propagation is switched the sign of the current also changes. Of note, this can be applied not only to opposite directions (positive or negative) but also any angle in between where the velocity of flow is off axis between the two positions. This thesis simulates reciprocity in the down current direction (positive effect), so to get the non-reciprocal result, the result needs to be doubled.

The conditions used will be the same geoacoustic model, as given in Table 1, of the ocean bottom found by Tan et al. [5]. The processes used will be to develop an effective sound speed profile (ESSP) based on realistic data from the Florida Straits and then use inversion to develop the velocity profile approximation. Afterward, the errors of approximation will be investigated as well as the required accuracy of measurement to achieve a useable depth-dependent velocity profile.

Table 1. Geoacoustic properties of the seafloor in the Florida Straits: Source: [5].

Sediment Thickness (m)	Sediment density (kg/m^3)	Sediment Sound Speed (m/s)	Basement Density (kg/m^3)	Basement Sound Speed (m/s)
14	1.40	1550	2.35	2375

These inputs, along with the desired frequency band and measured SSP (shown later in Figure 2) of the Florida Straits, are input into KRAKEN [10] and the modal group speed is output. This output was considered the background profile with normal mode

travel times concurrent with no flow. To find the ESSP, a current profile of a quarter wavelength of cosine was utilized as seen in Equation 2. This simulates realistic data in the Florida Straits as velocity profiles at this location typically are 0 m/s at the bottom to about 1 m/s at the surface.

$$v_0(z) = u_0 \cos(\frac{\pi z}{2}) \tag{2}$$

Equation 2 is the velocity profile of the test case used to determine the ESSP. The velocity profile is dependent on depth z and initial velocity u_0 such that the max current at the surface is 1 m/s and 0 m/s at the ocean floor. The horizontal current (Equation 2) is then added to the original SSP to obtain the ESSP. The visual representation of the ESSP is shown in Figure 2.

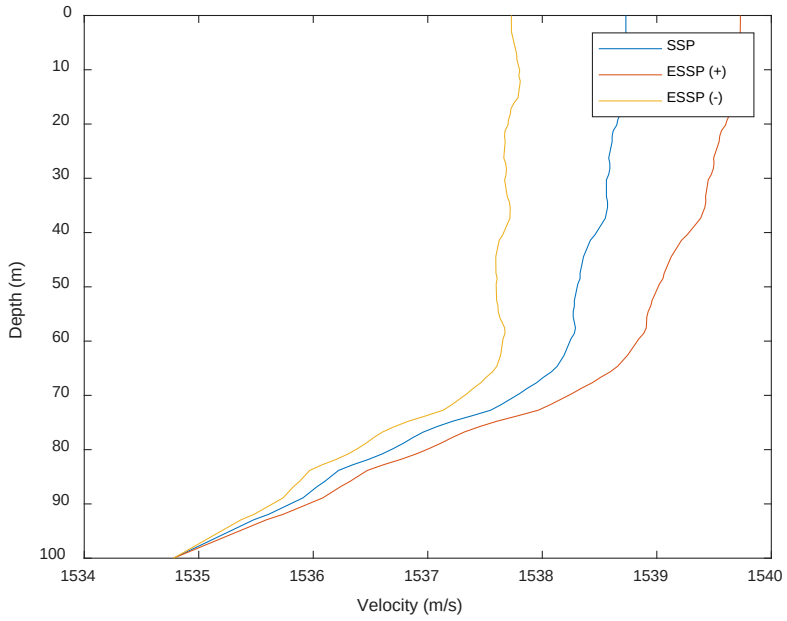

Figure 2. SSP and ESSP with current in the down current (+) and up current (-) directions.

The small differences between the background SSP and ESSP dispersion curves indicate small but measurable perturbations in the group speed, as shown in Figure 3. From Figure 3, we see a dependence of mode and frequency on the dispersion for each frequency. It can then be inferred that different modes are affected differently at separate frequencies.

This difference will be quantified in the results chapter and used to approximate the original velocity profile.

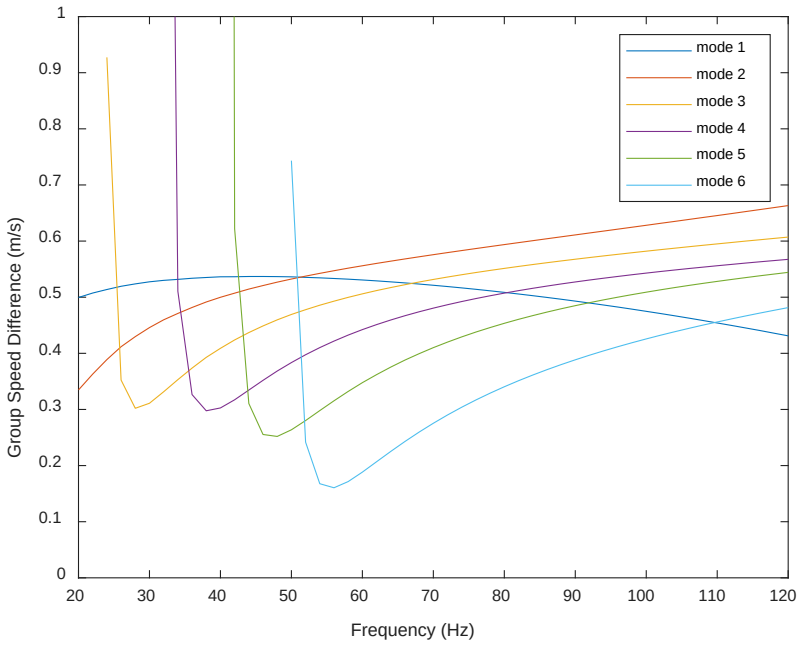

Figure 3. Calculated difference between the two profile dispersion curves of normal modes for the first six modes.

B. LINEAR INVERSION

To ensure that the data is in fact linear we can test multiple magnitudes of current profiles and verify we retrieve the same dispersion curve perturbations differing only by the same magnitude. To test this, current profiles with the shape of the quarter wavelength of cosine as stated in Equation 2 with magnitudes 0.5 m/s, 1 m/s, and 2 m/s were compared. As seen in Figure 4, the dispersion curves of 1 m/s and 2 m/s were 2 times the magnitude of 0.5 m/s and 1 m/s, respectively. To further see the comparison in Figure 5 0.5 m/s is scaled directly onto 1 m/s and 1 m/s onto 2 m/s by multiplying the smaller value by two. From this the scaled 0.5 m/s lines up pretty well with 1 m/s, but 1 m/s scaled to 2 m/s starts to shows some deviation from linearity. Thus we can conclude that our system is in fact linear for small perturbations; but, as larger currents are used, linearity begins to break down. As less than 2 m/s of current is realistically what could be expected in the Florida Straits, we are safe from this issue.

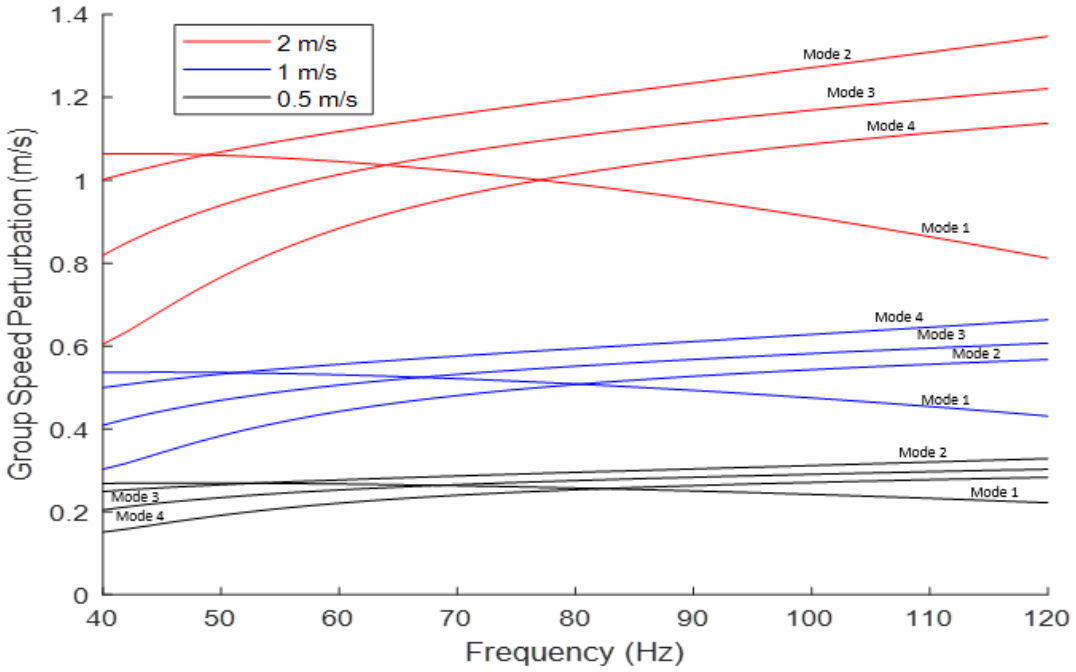

Figure 4. Plot of modes 1–4 of perturbation in the group speed vs. frequency for velocity profile magnitudes of 0.5 m/s (black), 1 m/s (blue), and 2 m/s (red).

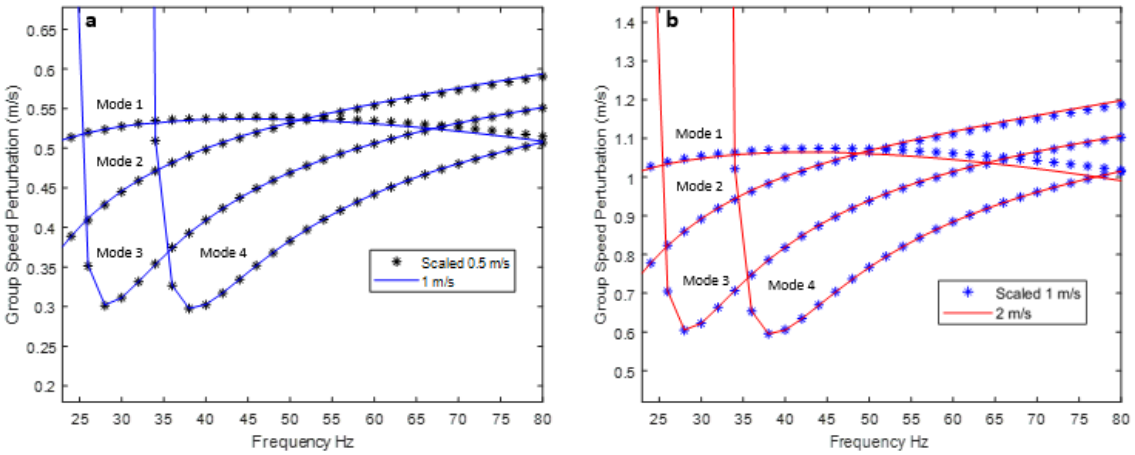

(a) Perturbations of the group speed of 0.5 m/s scaled by 2 (stars) compared to perturbations of 1 m/s (blue line) and (b) perturbations of the group speed of 1 m/s (stars) scaled by 2 compared to perturbations of 2 m/s (red line).

Figure 5. Scaled perturbations of the group speed of scaled 0.5 m/s and scaled 1 m/s compared to 1 m/s and 2 m/s, respectively.

As the system is confirmed to be linear, as long as currents are not much higher than 2 m/s, then we can use linear inversion as an applicable method to solve the inverse problem as in chapter 6 of [6]. As an added benefit, this method will save on computing time and effort. The goal is to use the weighted sum (linear combination) of basis functions as a means to approximate the solution and only conduct a set number of calculations vice the hundreds necessary with non-linear methods. Therefore, to solve we need to approximate the current profile by means of minimizing the norm of the goodness of fit, otherwise known as a cost function. Equation 3 is the measure of error, or measure of the mismatch, using the least squares method.

$$\Phi\left(\alpha_1,\alpha_2,\ldots,\alpha_N\right)=\left(\mathbf{D}-\sum_{n=1}^{N}\alpha_n\mathbf{m}_n\right)^2+\beta\mathbf{D}\cdot\mathbf{D}\sum_{n=1}^{N}\alpha_n^2 \tag{3}$$

$$\mathbf{D}=\left(U_1(f_1),U_1(f_2),\ldots,U_1(f_K),U_2(f_1),\ldots,U_M(f_1),U_M(f_2),\ldots,U_M(f_K)\right) \tag{4}$$

In Equation 3, Φ is the measure of the mismatch between **D** and the linear combination of α_n $\mathbf{m}_n$. **D** is a vector of data of the perturbations between the test and background profiles for all frequencies and modes as given by Equation 4. Model vectors used to approximate the test profile are given by $\mathbf{m}_n$. β is a value greater than zero and much less than one to ensure stability of the solution. In short, the term β does not allow for eigenvalues of zero to exist such that the inverse of the correlation matrix A, which will be defined later in the basis functions section, will exist.

To ensure minimization of the errors we find the partial derivatives of Φ with respect to α_j and set them equal zero. Thus our resultant formula to minimize the errors in matrix notation is given in Equation 5. From here, we need to solve for the vector $\vec{\alpha}$ to achieve the optimal weights of each basis function.

$$\hat{A}\vec{\alpha}=\mathbf{b}^T \tag{5}$$

In Equation 5, **A** is N×N matrix with elements a_{jn} ; $\vec{\alpha}$ = (α1,…, αN) and **b** = (b1,…, bN) are N-dimensional vectors; and T denotes the transpose, where vectors $\mathbf{b}_j$ and matrix components a_{jn} are given by equations 6 and 7.

$$b_j = \mathbf{m}_j \cdot \mathbf{D}, \quad a_{jn} = \mathbf{m}_n \cdot \mathbf{m}_j + \beta \mathbf{D} \cdot \mathbf{D} \delta_{jn} \tag{6}$$

$$\begin{aligned} \mathbf{m}_j = \big(&\delta u_1^j(f_1), \delta u_1^j(f_2), \ldots, \delta u_1^j(f_K), \delta u_2^j(f_1), \delta u_2^j(f_2), \ldots, \delta u_2^j(f_K), \\ &\ldots, \delta u_M^j(f_1), \delta u_M^j(f_2), \ldots, \delta u_M^j(f_K)\big) \end{aligned} \tag{7}$$

The value a_{jn} is the dot product of the basis functions n and j added to the stability function. The term $\delta u_M^j(f_K)$ represents the basis function's frequency dependence on measured non-reciprocities in travel times of normal modes where j is the basis function and M is the mode. Each value of a_{jn} construct the matrix **A**, which is the correlation of each basis function to each other. If the dot product is zero for any of these two vectors, then the Kronecker delta function, δ_{jn}, will be one resulting in the addition of the $\beta \mathbf{D} \cdot \mathbf{D} \delta_{jn}$ term. This ensures that the inverse of **A** will exist.

From here, we can solve for the coefficient vector $\vec{\alpha}$ to achieve our solution to the optimization problem Equation 8.

$$\vec{\alpha} = \hat{A}^{-1} \mathbf{b}^T \tag{8}$$

C. BASIS FUNCTIONS

The basis functions consist of the six power functions as seen in Table 2 where x is defined by Equation 9. The power functions were initially chosen due to their likeness to the velocity profile of 0 m/s at the bottom as we would see in the Florida Straits. Each function is treated as a separate velocity profile just as the test case of the quarter wavelength of cosine. With the six basis functions, j different ESSPs are generated. The difference between the ESSP's and background's group speed was taken to get the frequency-dependent perturbation vector of the group speed for each ESSP. Thus $\mathbf{m}_j$ for j=1,2,…,6 represents each ESSP and then used to develop the correlation matrix **A**.

Table 2. Basis Functions 1 through 6. Each basis function represents a different velocity profile used to create six different ESSP. A weighted linear combination of the six will result in approximation of the current profile.

1	$1-x$	$(1-x)^2$	$(1-x)^3$	$(1-x)^4$	$(1-x)^5$

$$x = -1 + 2\left(\frac{z}{D}\right) \tag{9}$$

Equation 9 is the definition of x for the basis functions such that x is -1 at the surface and 1 at the sea floor. The variable *z* is the depth from 0 to 100 meters and *D* is the total depth. This ensures that the velocity profile of each basis function will be 1 m/s at the surface and 0 m/s at the bottom.

As discussed by Dr. Tan et al., from the data available in the Florida Straits, it is harder to identify higher order modes which in turn limits the ability of basis functions to make adequate approximations [5]. Six basis functions were chosen as previous experience with accuracy of data suggests a need to limit the number of basis functions. To quantify the ability of the number of functions used to approximate the current profile, the root mean square error (RMSE) was found, as shown in Table 3, for a frequency band of 20–200 Hz with the first four modes between the approximated profile and test profile of a quarter wavelength of cosine.

Table 3. RMSE for using three to eight basis functions using frequency band 20–200 Hz and first four modes for calculation.

Number of Functions	**RMSE (m/s)**
3	0.0151
4	0.0149
5	0.0143
6	0.0138
7	0.0132
8	0.0128

From Table 3, although seven and eight functions do give slightly better approximations, six functions are ideal; fewer functions do not contain the desired accuracy of approximation, and the limitations of using higher orders, including increased computing time, need to be avoided. Therefore, six functions is chosen for this model.

Additionally, the basis functions need to be ensured that they are adequate to model the solution. For this it must also be confirmed that the matrix **A** is symmetric positive definite. This will also imply that a unique solution exists. **A** will be a positive definite matrix if all eigenvalues are positive and thus invertible. From basic operations of the dot product calculations and Table 4 matrix **A** is symmetric. In Table 5, a frequency range of 20 to 200 Hz with six modes, all eigenvalues of **A** are positive. Thus our basis functions are adequate to approximate the solution.

Table 4. Matrix **A**, the correlation matrix. The matrix is calculated for the first six modes in the frequency band from 20 to 120 Hz.

554.57	539.99	712.56	1082.44	1827.66	3576.86
539.99	529.905	703.48	1073.38	1818.53	3568.75
712.56	703.48	938.88	1438.49	2445.66	4815.78
1082.44	1073.38	1438.49	2213.01	3779.63	7485.22
1827.66	1818.53	2445.66	3779.63	6494.97	12976.88
3576.86	3568.75	4815.78	7485.22	12976.88	26294.24

Table 5. Eigenvalues of matrix **A.** Eigenvalues of matrix **A** are all positive indicating the matrix is a positive definite matrix. Matrix **A** is based on frequency band of 20 to 200 Hz, using the first six modes for calculation.

$\boldsymbol{\lambda}_1$	0.000491
$\boldsymbol{\lambda}_2$	0.0750
$\boldsymbol{\lambda}_3$	0.404
$\boldsymbol{\lambda}_4$	18.6
$\boldsymbol{\lambda}_5$	246
$\boldsymbol{\lambda}_6$	36800

III. RESULTS

A. NORMAL MODE TRAVEL TIME

The analysis conducted analyzes the effect of currents on the acoustic field in terms of non-reciprocity of group speeds. In practice, these characteristics in the acoustic field are typically measured directly by non-reciprocity in the normal mode travel time. The change in the group speed can be directly related to changes in the normal mode travel time. The method used in this thesis only deals with one direction and since perturbations in the travel times are measured from both directions, then the final travel time described by this method is only half of the actual value due to non-reciprocity. Calculation of the difference in travel time between a moving and motionless fluid, is given by Equation 10.

$$\Delta t = \frac{-r}{v_g^{\,2}} \delta v_g \tag{10}$$

In Equation 10, r is the range between receivers, which is assumed to be 5 km just as in the Straits of Florida experiment [7]. The group speed is given by v_g and δv_g is the group speed perturbations. So, at 30 Hz, mode 1's group speed is 1519.3 m/s and the change in the group speed from the background profile is 0.1576 m/s yields the result of 0.341 s. As stated before, this is only half of the change in travel time due to current, so the total change in travel time due to non-reciprocity of up and down current is 0.682 ms.

B. INVERSION ERROR DEPENDENCE ON FREQUENCY BAND AND NUMBER OF MODES

The frequency band and number of sequential modes used to calculate the approximation of the depth-dependent current profile affects the accuracy of results. To determine the appropriate frequency band and number of sequential modes needed, several groupings were used. The first goal was to reduce the difference between the profile retrieved from inversion and the actual velocity profile. The bands used were 20 to 120 Hz, 20 to 200 Hz, 20 to 80 Hz, and 50 to 80 Hz. For each frequency band, the number of modes used for the calculations started with the first three sequential modes and adds each

sequential mode from there (e.g., first three modes, first four modes). To determine the goodness of fit, depth-averaged root mean square error (RMSE) and depth-dependent error were calculated and compared for each band and number of modes used. For clarity, the depth-averaged RMSE is defined as the standard deviation of residuals and the depth-dependent error is described as the difference between the approximated profile from inversion and the actual current velocity profile. The second goal was to prove that the basis functions could also adequately approximate profiles other than the simple cosine profile. For this test, actual averaged current profile data form the Florida Straits was used.

For the frequency band of 20 to 120 Hz, the first three to fourteen sequential modes were tested. As sequential modes are used the RMSE decreased until ten modes were used and then began to increase with each additional mode as seen in Table 6. A graphical representation is given in Figure 6.

Table 6. 20 to 120 Hz RMSE for the first three through fourteen modes.

# of Modes	RMSE (m/s)
3	0.0151
4	0.0126
5	0.0091
6	0.0084
7	0.0084
8	0.0084
9	0.0082
10	0.0083
11	0.0173
12	0.0173
13	0.0173
14	0.0156

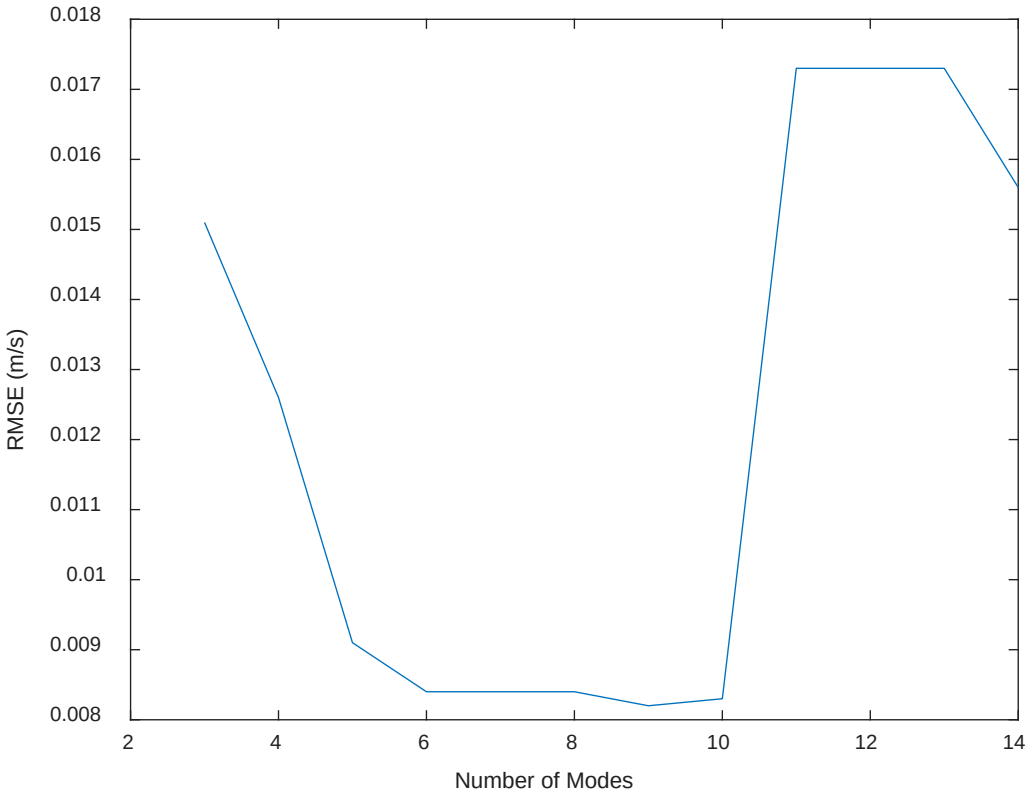

Figure 6. Depth-averaged RMSE versus sequential modes three through fourteen for frequency band 20 to 120 Hz.

From Table 6 and Figure 6 we can conclude that the use of the first six modes through the first ten modes seem to be the most optimal with nine modes being the best for a frequency band of 20 to 120 Hz. Therefore, for a frequency band of 20 to 120 Hz, with the first nine modes would be the best option.

The next test was to increase the upper limit of the frequency band to see if the higher frequencies may deliver more information. Table 7 shows the RMSE for the first three through fourteen sequential modes and a frequency band of 20 to 200 Hz. Figure 7 is Table 7 in graphical form.

Table 7. 20 to 200 Hz RMSE for first three through fourteen sequential modes.

# of Modes	RMSE (m/s)
3	0.0140
4	0.0138
5	0.0128
6	0.0120
7	0.0114
8	0.0113
9	0.0114
10	0.0114
11	0.0124
12	0.0124
13	0.0123
14	0.0123

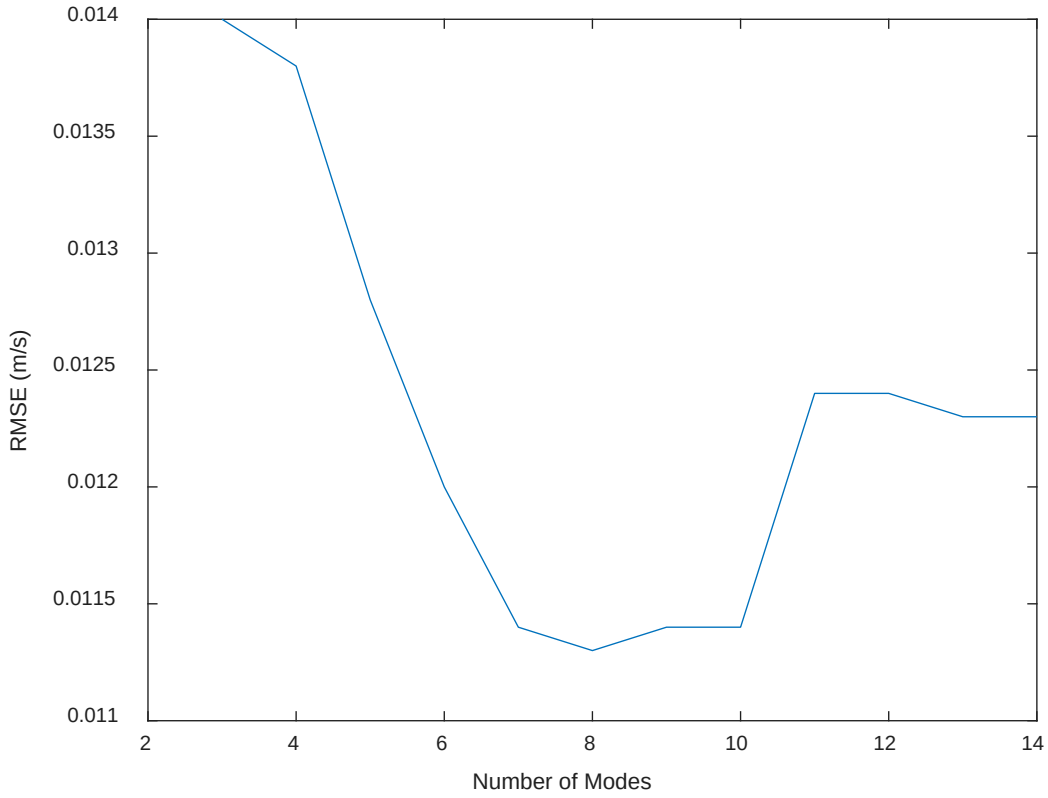

Figure 7. Depth-averaged RMSE versus number of first three through fourteen sequential modes for frequency band 20 to 200 Hz.

As it is easily seen the band of 20 to 200 Hz, as compared to 20 to 120 Hz, shows a little more error. Thus we can conclude that regardless of how much higher than 120 Hz the upper bound of the frequency band is set, the error will not decrease. This makes intuitive sense as all modes converge to the sound speed in the medium for higher frequencies. Therefore, the frequency band of 20 to 200 Hz does not provide any better information than using the much narrower band of 20 to 120 Hz. Since 20 to 200 Hz requires more computing time due to the increased group speed calculations and no discernable benefit to the final approximation, preference should be towards a lower frequency band such as 20 to 120 Hz.

Due to the fact that the upper limit of the 200 Hz band was too high, it was then investigated if 120 Hz was also too high of an upper bound for the frequency band. To test this a frequency band of 20 to 80 Hz for the first three through nine sequential modes. Less modes are used than previously as the cutoff frequency for these modes is higher than the upper band limit. Table 8 is a table of the RMSE for this band and Figure 8 is the graphical representation. From this we see that the lower upper bound is indeed better as RMS levels are much lower. Also, nine modes appears to be the optimal number of sequential modes to use to reduce overall error.

Table 8. 20 to 80 Hz RMSE for the first three through nine sequential modes.

# of Modes	RMSE (m/s)
3	0.0122
4	0.0094
5	0.0059
6	0.0065
7	0.0060
8	0.0060
9	0.0046

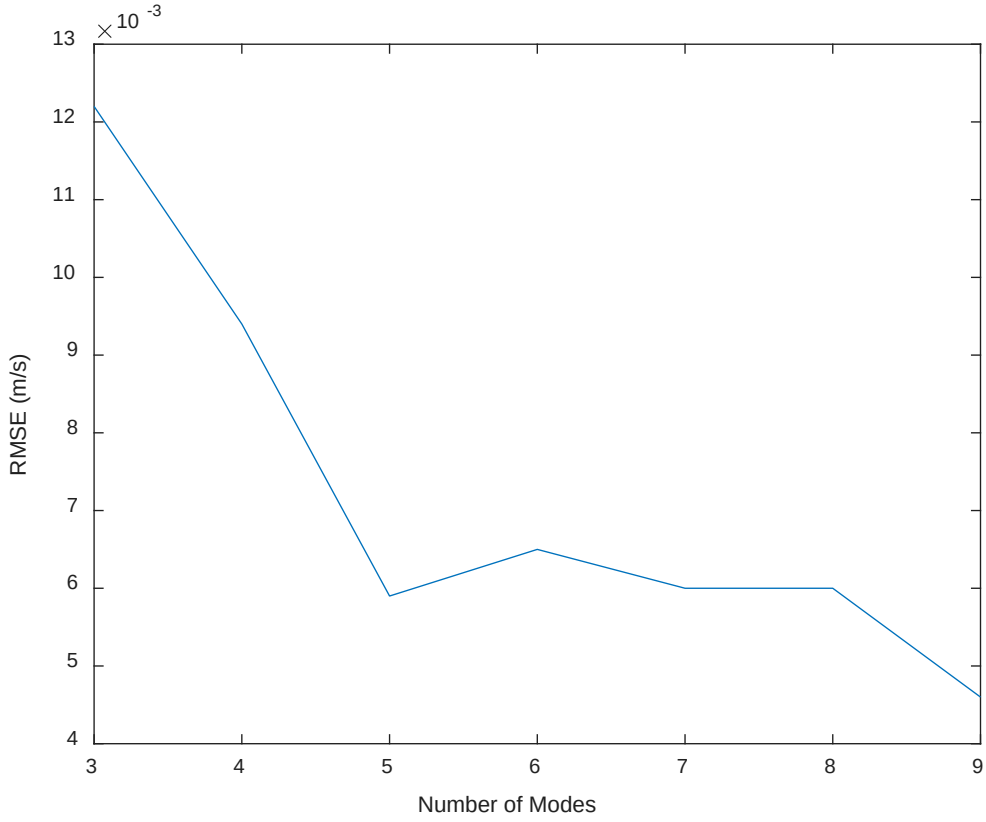

Figure 8. Depth -averaged RMSE versus mode for frequency band 20 to 80 Hz for the first three through nine sequential modes.

Finally, a check needed to be conducted with a higher lower bound. To test this, a much narrower frequency band of 50 to 80 Hz was used. As Table 9 and Figure 9 show, the 50 to 80 Hz band has similar characteristics; however, the depth-averaged RMSE value for higher modes were slightly smaller leading up to 9 modes than that of the 20 to 80 Hz band. This suggests that it is possible the 50 to 80 Hz band is better than 20 to 80 Hz; but, once we look at the depth-dependent error, which is determined from the difference between the approximated profile obtained from inversion and the actual profile, we see a different case (Figure 10).

Table 9. 50 to 80 Hz RMSE for the first three through nine sequential modes.

# of Modes	RMSE (m/s)
3	0.0270
4	0.0113
5	0.0143
6	0.0043
7	0.0050
8	0.0046
9	0.0046

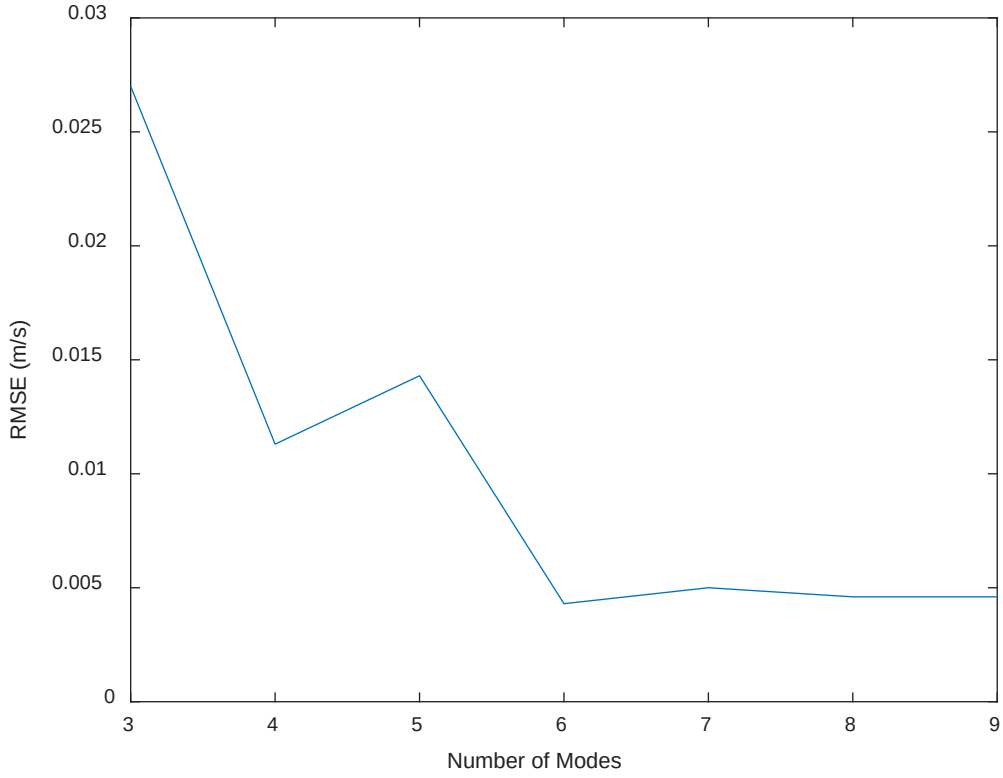

Figure 9. Depth-averaged RMSE versus mode for frequency band 50 to 80 Hz for modes three through nine.

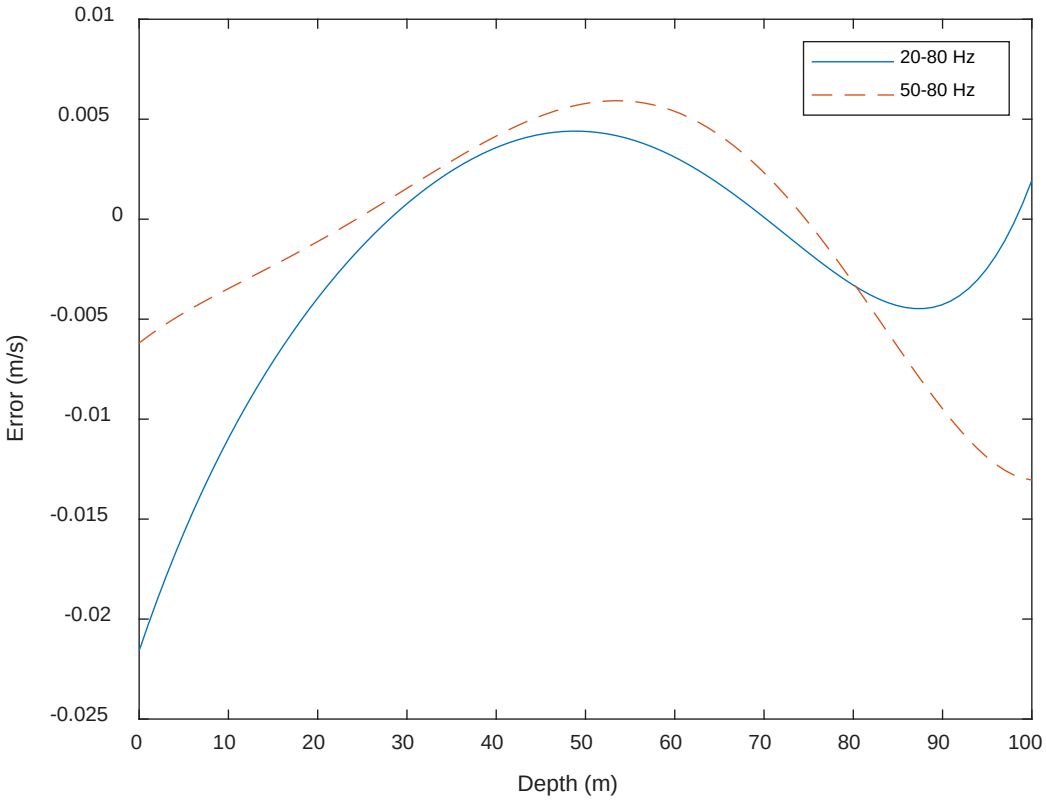

Figure 10. Depth-dependent error for 20 to 80 Hz (blue line) and 50 to 80 Hz (dashed orange line) versus depth

From Figure 10 it can be seen that even though the depth-averaged RMSE values for the 50 to 80 Hz band are low like 20 to 80 Hz, the depth-dependent errors show that the error grows with depth in the narrower band of 50 to 80 Hz. This is far from ideal as the accuracy of the approximation is depth-dependent such that it gets less accurate with greater depth. If other depths are used, as the medium gets larger, the RMSE and depth-dependent error will continue to increase to the point that 20 to 80 Hz would be a better frequency band. For this reason, the frequency band of 20 to 80 Hz is still the ideal band to use.

The next step is to test that the linear approximation method can solve for other profiles as well. For this test, a measured current profile from the Florida Straits as was investigated in an article in the *Journal of Physical Oceanography* by Winkel et al. was used [11]. As adapted from their study, Figure 11 shows the velocity profile that was

collected from multi-scale profiler (MSP) station 2. The light lines are individual collections of velocity profiles throughout the day and heavy lines indicate the average profile. The data set used for this test was that of the second set of data collection on 11 June 1990. Even though this data taken from MSP station 2 is in a different area with a different maximum depth than that of the 2012 Florida Straits experiment, it is close enough to give an idea of what the current velocity profile would look like. To adjust this profile to fit in the depth used for this experiment, the velocity profile gathered was scaled from 0 to 380 meters to 0 to 100 meters and the current velocity was interpolated to be zero at the bottom as seen in Figure 12. Figure 12 also contains the velocity profile approximation from inversion, in the down current direction, as to make direct comparison of the approximation to the actual velocity profile.

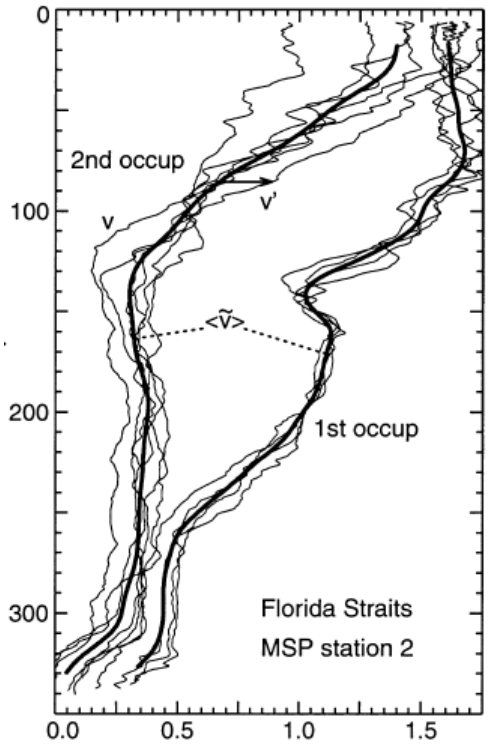

Thin lines represent collection of data throughout the day and thick lines represent the average profile for the whole day.

Figure 11. Velocity profile of the Florida Straits in vicinity of MSP station 2 as adapted from Winkel et al. [11].

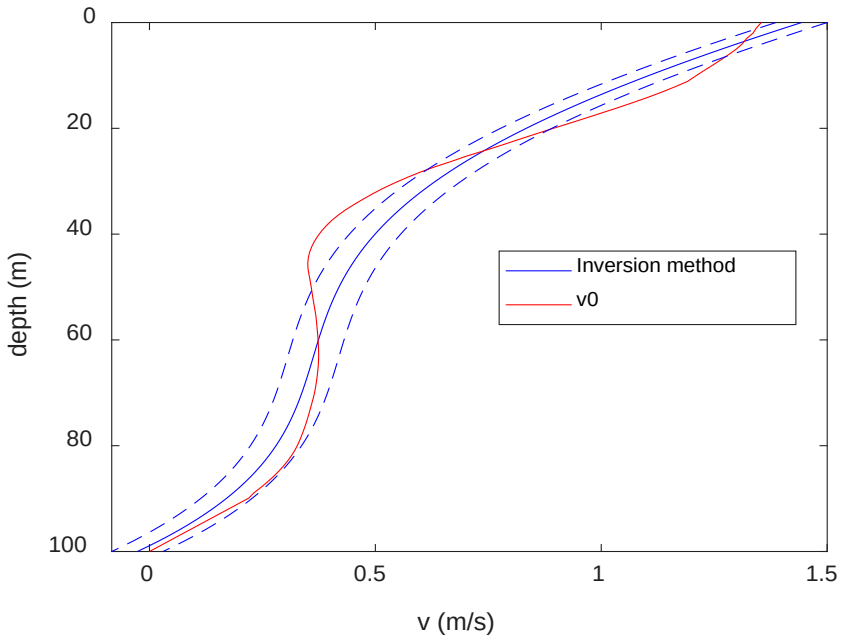

The blue line is the solution of the inverse problem. The red line indicates the scaled velocity profile as gathered from the Florida Straits. The dashed lines are the +/- depth-averaged absolute value of deviation.

Figure 12. Comparison of the resultant passive acoustic solution from inversion and scaled current velocity profile data from [11] in the Florida Straits.

As seen in Figure 12, the linear inversion approximation of the velocity profile is marginal and leaves room for improvement with a depth-averaged RMSE of 0.0567 m/s. As stated by Winkel et al. [7], the Florida straits have very strong and complex currents and this profile begins to approach the breakdown of linearity. Though the basis functions work well for simple profiles that remain below velocities of 2 m/s more complex profiles such as those seen in the Florida Straits require a more diverse and orthogonal set of functions. This opens up further opportunities for research into alternate basis functions utilizing the same numerical methods as provided in this thesis to provide a better fit for the data.

C. EFFECTS OF MEASUREMENT ERRORS ON RESULTS OF INVERSION

Now with the optimal frequency band of 20 to 80 Hz measured with nine modes, the approximation through linear inversion is as close as possible. From this point we can

investigate the effect of measurement error of the group speed on our ability to obtain an acceptable velocity profile approximation through linear inversion. For the purposes of this test, 10% is used as an arbitrary measure of acceptable percent deviation based on the depth-dependent RMSE and depth-dependent error of the mean. The depth-dependent RMSE is based on standard deviation of the residuals of each individual measurement and the depth-dependent error of the mean is the difference between the mean inversion profile and actual profile at each depth. The quarter wavelength of cosine test profile is used again to model a theoretical current profile for the simple case.

There are two viable methods to simulate the experimental situation in which multiple measurements of the group speed are taken with random error. The first is to measure the group speed and then conduct inversion for each instance and then average these inversions together to get the mean profile. Alternatively, by averaging the different measurements of the group speed and then conduct inversion only once, this average will yield the same results as a nice benefit due to linearity.

Therefore, to model this simulation of measurement error in the group speed, a random distribution with a mean 0 m/s and variances between 0 to 0.5 m/s were applied to each frequency's group speed. In order to ensure sufficient data, 30 trials are used as seen in Figure 13 (a). In Figure 13 (a), the standard deviation of the measurement error used was 0.10 m/s. To get the approximated profile these 30 trials were then averaged to get the mean approximated profile to be compared to the test profile we are trying to get. As we will later see, by averaging these 30 different trials, the final accuracy of measurement greatly increases. Thus to maintain favorable results of approximation many measurements of the group speeds need to be averaged together to ensure measurement error is minimized rather than just one individual measurement. Alternatively, we could take the average of the group speed errors first and then only conduct the inversion once as discussed earlier and as seen in panel (b) of Figure 13.

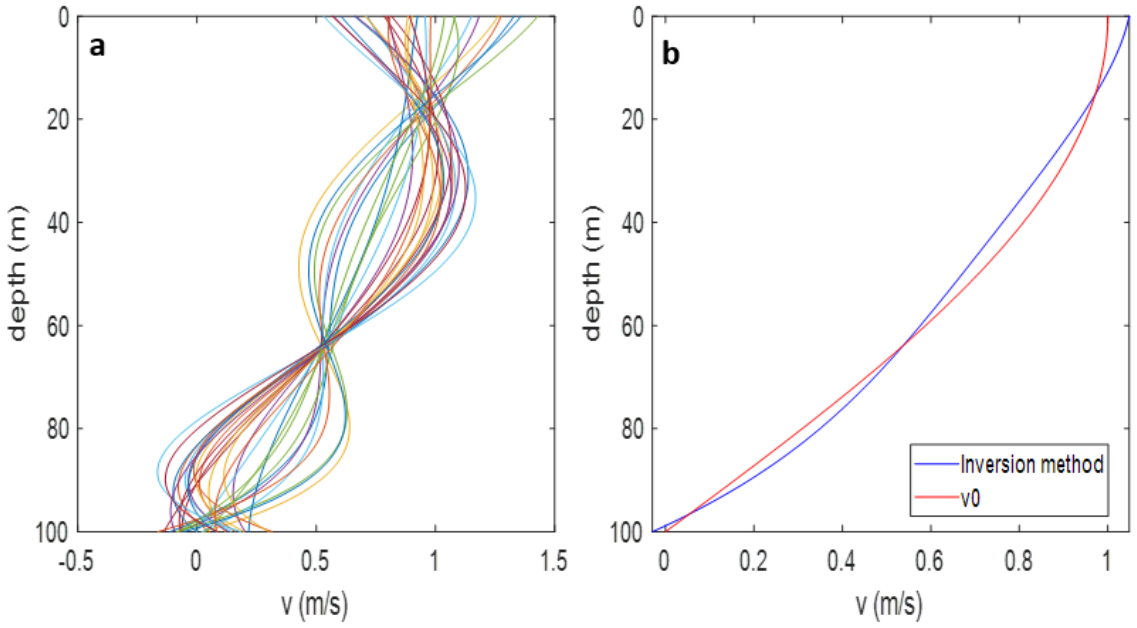

(a) 30 profiles based on random measurement error. (b) Inversion of the average of 30 measurements compared to the cosine profile.

Figure 13. Resultant velocity approximations of 30 random trials of a measurement error of 0.1 m/s deviation for the quarter wavelength of cosine.

The graphical representations with no measurement error (0.0 m/s) are shown in Figure 14. The approximation has minimal RMSEs and the error of the mean inversion remains close to 0 m/s for all depths. This will be used as a reference as additional measurement error is introduced.

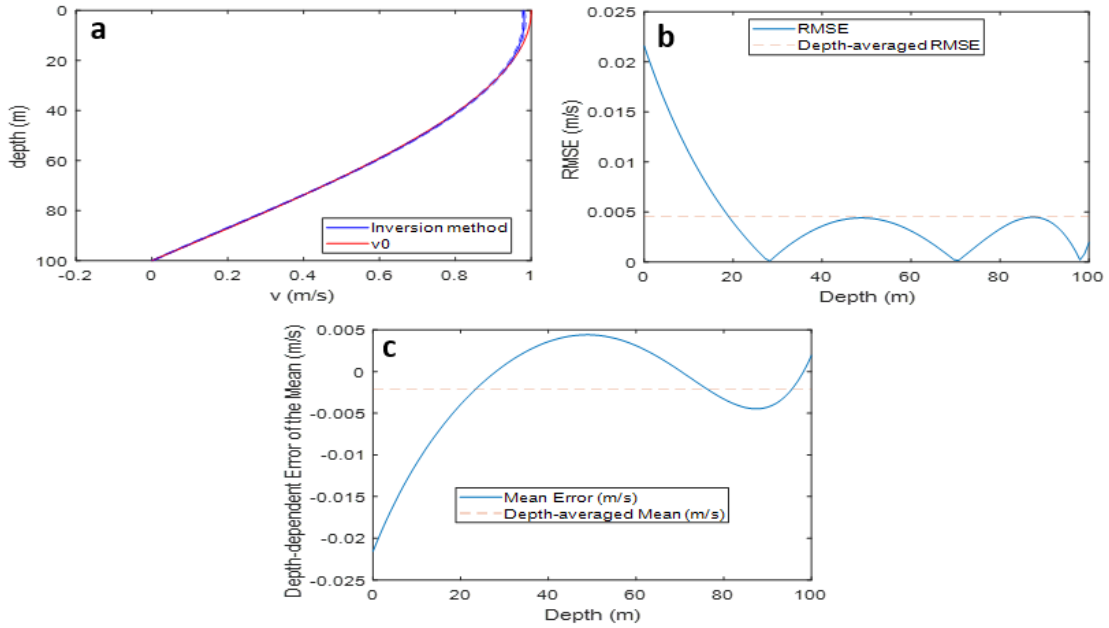

(a) The resultant velocity approximation against the quarter wavelength of cosine profile, (b) depth-dependent RMSE, and (c) depth-dependent error of the inversion of the mean of 30 random measurements.

Figure 14. Error analysis of the inverted profile with no measurement error.

As the measurement error is increased the accuracy of the inverted profile steadily decreased. When the measurement error is 0.10 m/s we start to see the average RMSE approach 15%, above our upper limit of acceptable error as seen in Figure 15 part (b) for individual measurements. When the measurement errors are averaged over the 30 trials we receive an adequate approximation of at most an error of the mean of 2% for any depth with the depth-averaged error very close to 0 m/s like in Figure 15 part (c). Thus we see the value in averaging over multiple measurements, as this is the best way to reduce errors.

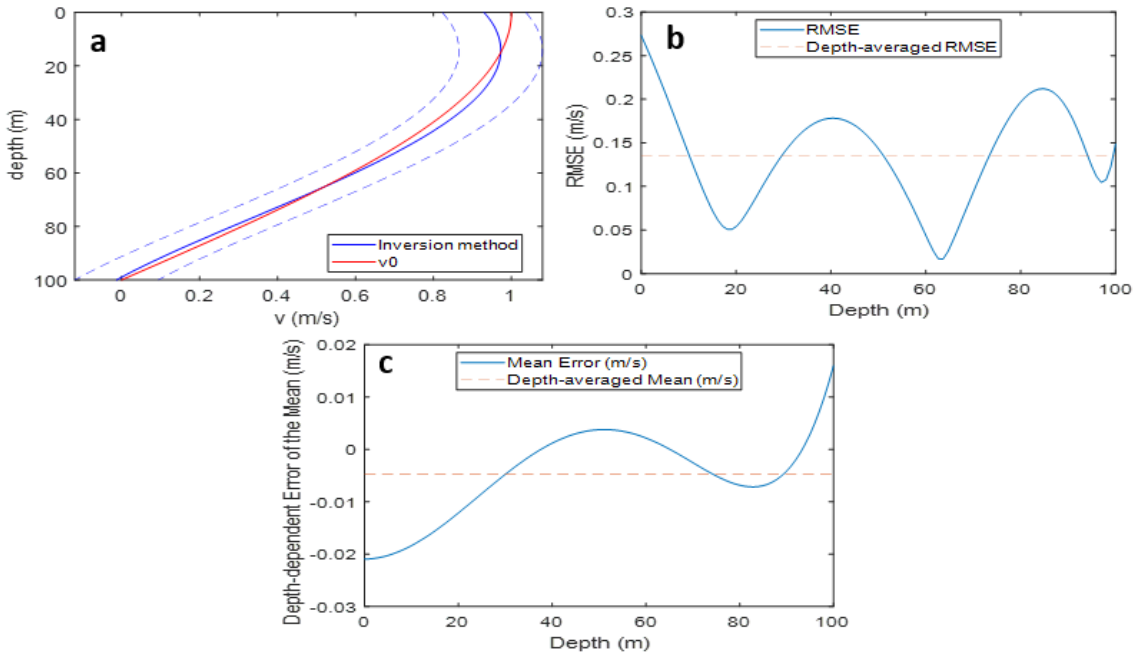

(a) The resultant velocity approximation against the quarter wavelength of cosine profile, (b) depth-dependent RMSE, and (c) depth-dependent error of the inversion of the mean of 30 random measurements.

Figure 15. Error analysis of the inverted profile with 0.10 m/s measurement error.

In Figure 16 part (b) we see the effect of too large of a measurement error of 0.2 m/s, resulting in about 30% RMSE for the individual errors; however, by averaging over 30 different measurements we still keep the depth-dependent error of the mean to below 10% for all depths with the depth-averaged error of the mean very close to 0. Since we are most concerned with finding the depth-dependent current velocity profile, the measurement error of 0.20 m/s is the maximum allowable error due to the depth-dependent error of the mean being close to 10% in the vicinity of 40 meters and 85 meters.

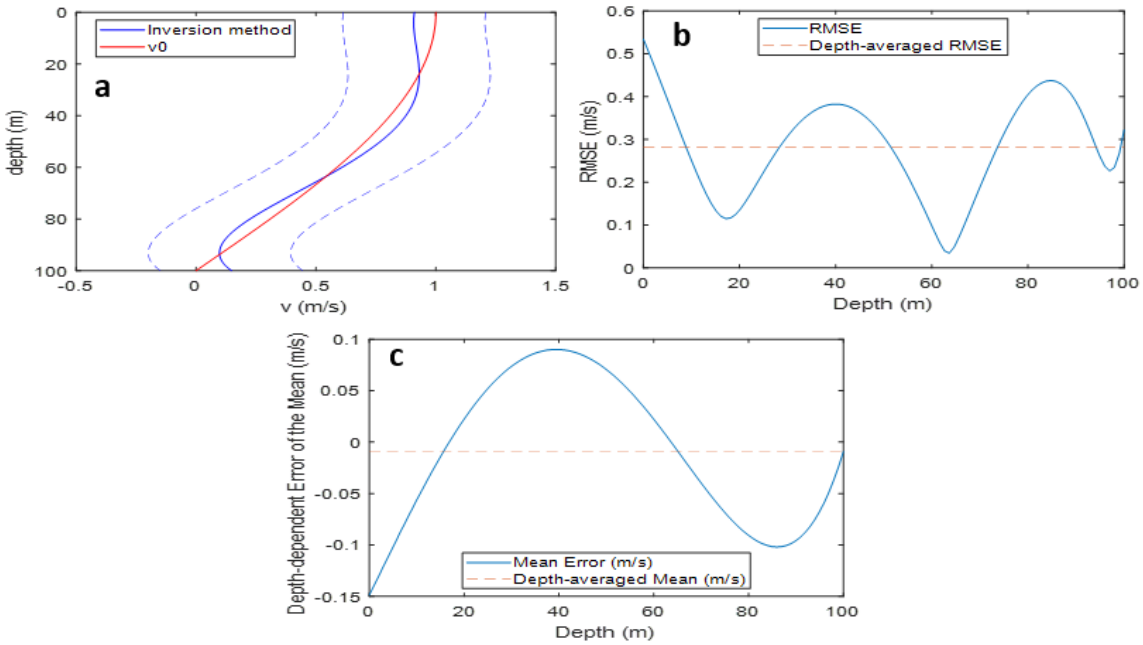

(a) The resultant velocity approximation against the quarter wavelength of cosine profile, (b) depth-dependent RMSE, and (c) depth-dependent error of the inversion of the mean of 30 random measurements.

Figure 16. Error analysis of the inverted profile with 0.20 m/s measurement error.

Figure 17 shows the average RMSE and maximum RMSE for each measurement error. The average RMSE is based on the mean value of the 30 trials of each measurement error. The max RMSE is the maximum value of the individual RMSEs used in the 30 trials. As we would expect the RMSE increases with increasing measurement error. Of note, we see that the RMSE for each measurement, begins to diverge faster after 0.20 m/s. This further displays that the group speed needs to be measured to an accuracy of about 0.20 m/s for a simple velocity profile, otherwise we will be unable to approximate adequately for situations where we only deal with inversion of a single measurement.

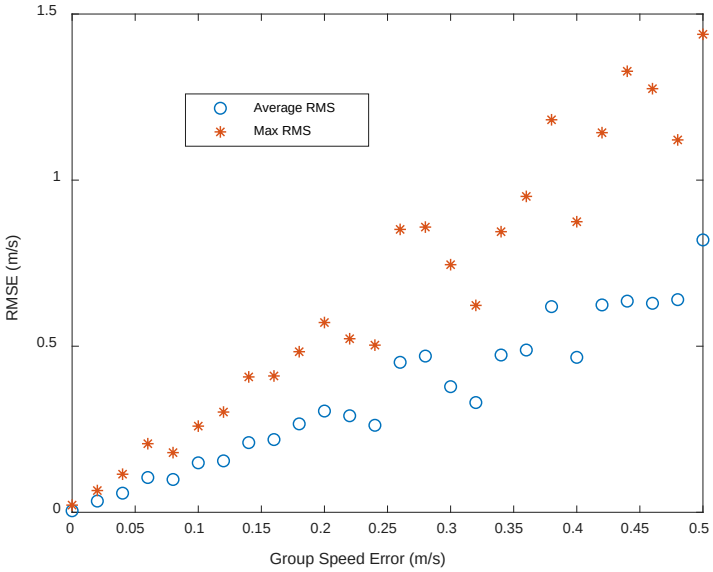

Figure 17. Dependence of depth-averaged RMSE on group speed measurement error. The circles are depth-averaged RMSE and the stars are maximum RMSE deviation present over 30 random trials.

Returning to the real Straits of Florida current velocity profile discussed in Figure 11 and 12, there is not as much room for measurement error as was seen in Figure 12 since it is already halfway to our limit of overall 10% depth-averaged error. Though, to check the robustness of the approximating method it was investigated how much measurement error would make the results considerably worse. In Figure 18, the first measurement error of 0.02 m/s is shown. From this we see that even though the accuracy of the approximation is far from ideal, this small measurement error barely brings the RMSE over 0.06 m/s with a depth-dependent error of the mean at most of 12% with the depth-averaged error very close to 0. As such this is not a significant change from the original approximation, so our approximation is relatively strong for small measurement errors.

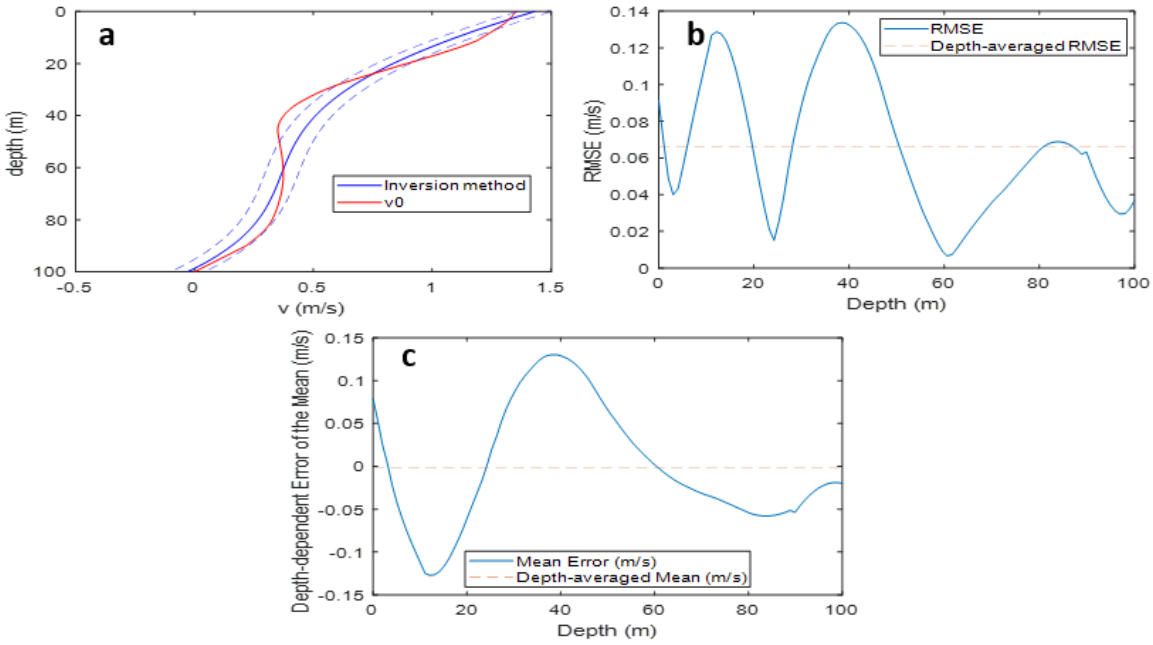

(a) The resultant velocity approximation against the actual profile, (b) depth-dependent RMSE, and (c) depth-dependent error of the inversion of the mean of 30 random measurements.

Figure 18. Error analysis of the inverted profile with 0.02 m/s measurement error.

Though the depth-averaged RMSE of approximation is quickly approaching 10%, it can be seen that the errors start to really strengthen after a measurement error of 0.10 m/s as seen in Figure 19. In Figure 19 the measurement error of 0.10 m/s results in a depth-averaged RMSE of nearly 15% and a depth-dependent error of the mean of just above 10% in the shallower portion of the profile.

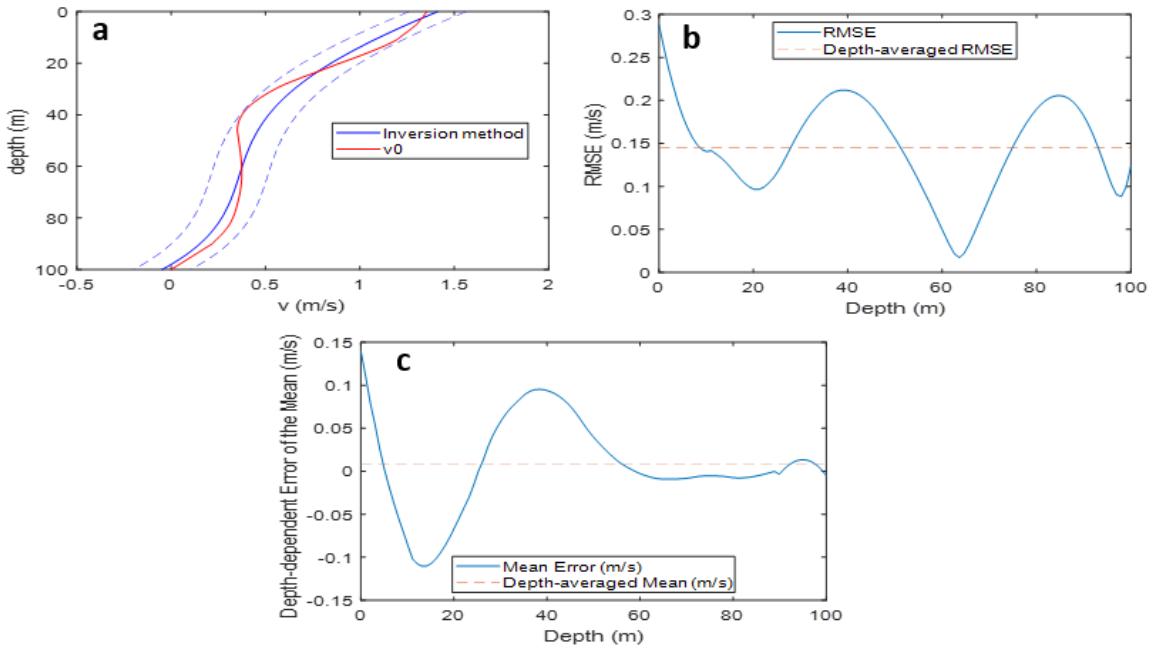

(a) The resultant velocity approximation against actual profile, (b) depth-dependent RMSE, and (c) depth-dependent error of the inversion of the mean of 30 random measurements.

Figure 19. Error analysis of the inverted profile with 0.10 m/s measurement error.

In Figure 20 the results are highly unfavorable as the depth-dependent RMSE is large and at more depths for a measurement error with deviation upwards of 0.20 m/s. The depth-dependent errors of the mean are well above 10% at several depths. This is the same pattern that was seen when trying to approximate the cosine profile. So if given better basis functions to approximate the current profile, it would still be important to remain below a measurement error of 0.20 m/s but with the current ability to approximate the more complex Florida Straits profile, 0.10 m/s should be the limit for an individual measurement.

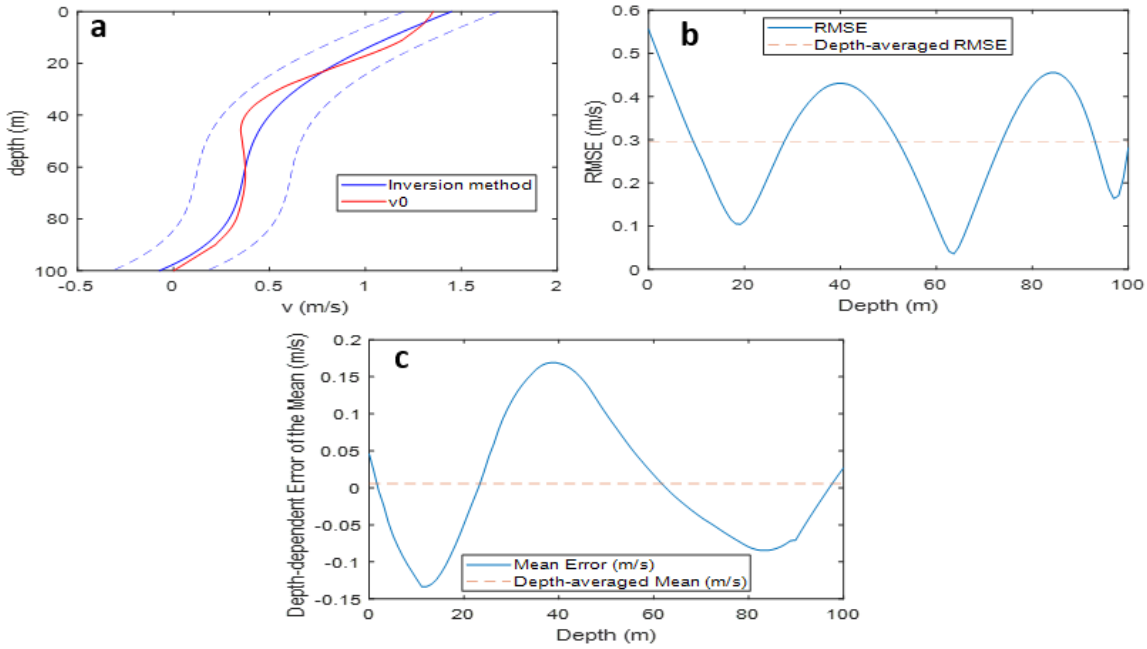

(a) The resultant velocity approximation against the actual profile, (b) depth-dependent RMSE, and (c) depth-dependent error of the inversion of the mean of 30 random measurements

Figure 20. Error analysis of the inverted profile with 0.20 m/s measurement error.

As before with Figure 17, Figure 21 shows the depth-averaged RMSE and maximum RMSE. The same pattern is seen of which the errors begin to dramatically increase after a certain measurement error, in this case 0.10 m/s. Thus even with the non-ideal approximation, the trend of errors remains the same, just more sensitive in this case. This further strengthens the conclusion that the group speed must be measured to an accuracy of 0.10 m/s for this more complex profile otherwise the compounding errors will result in poor approximations. Therefore, the complexity of the profile determines the level of accuracy of measurement needed. If the profile is relatively simple, 0.20 m/s would be a reasonable error. However, if a more complex such, as the profile measured from the Florida Straits, then a smaller error around 0.10 m/s would be tolerable for a single error but as stated previous, more measurements will increase the accuracy of the inverted profile.

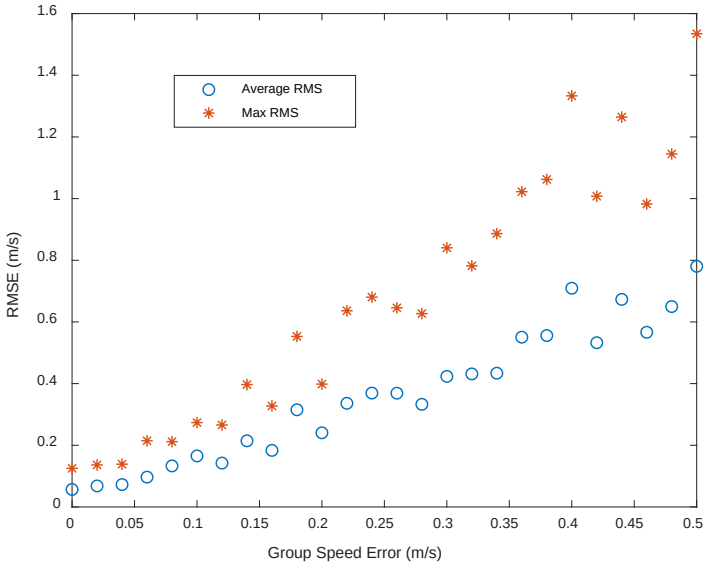

Figure 21. Dependence of depth-averaged RMSE on group speed measurement error. The circles are depth-averaged RMSE and the stars are maximum RMSE deviation present over 30 random trials.

Since the method of obtaining the group speed is found from the travel time between the two virtual transceivers it is necessary to use Equation 10 and relate these errors in the group speed to the allowable errors in travel times. Thus, the measurement error of 0.1 m/s to 0.2 m/s would relate to an error of travel time by about 0.217 ms to 0.433 ms in one direction. The non-reciprocity of the error in travel time due to both directions would then be in the range of 0.454 ms to 0.866 ms. This is an achievable accuracy of measuring travel time and still retain the ability to develop an accurate current velocity profile.

IV. CONCLUSION

Previous work by Godin et al. [7], Brown et al. [8], and Tan et al. [5]. discussed using the data gathered in the 2012 Florida Straits noise interferometry experiment to determine an extensive amount of oceanographic information from ambient diffuse noise alone. Depth-averaged current velocity and geoacoustic parameters of the seabed have been estimated. As an extension of that work, this thesis investigated the feasibility of retrieving the depth-dependent current velocity profile from two-point noise cross-correlation function assuming separation of acoustic normal modes via time-warping transform. In this work numerical experiments were used based on the geoacoustic properties, realistic current profile, and SSP gathered from the Florida Straits in previous experiments to determine the accuracy required in the measurement of the group speed of normal modes.

The quantitative results of this thesis determined that with reasonable measurement error of flow induced non-reciprocity of travel times of normal modes, the depth-dependent current velocity profile can be retrieved. With random measurement errors with deviation of 0.10 to 0.20 m/s in a single measurement, the inverted profile can accurately approximate the depth-dependent current velocity profile to within about 10%. Also, it was found that inverting the average of multiple measurements of the group speed non-reciprocity leads to a very significant suppression of the inversion error and allows one to considerably relax the requirements to the measurement accuracy. In addition, the linear inversion method discussed works well for the conditions of the Florida Straits. Another important result is that measurement in the frequency band, such as 20 to 80 Hz where non-reciprocity can be measured passively using noise interferometry, proves sufficient for retrieval of the current velocity profile provided that separation of normal modes is possible through time warping as in [5]. Thus, it follows that the technique studied in this thesis can now be applied to field data, like that retrieved in [7] and [8], with accuracy achieved in the previous time warping study by Tan et al. [5]. The results of numerical simulations also allow to quantitatively relate travel time measurement errors to uncertainty in the inverted profile.

Further research needs to be conducted to optimize retrieval of the velocity profile from passive measurements of acoustic non-reciprocity. Additional investigation of the frequency bands is required to develop the information different frequency ranges can provide as the set of four frequency bands used in this thesis is not sufficient to confirm the optimal frequency range for this specific application. In addition, other basis functions should be attempted to find a more accurate and robust approximation of the current profile in order to approximate more realistic profiles with more structure such as in the Florida Straits. The next step in this research is to use experimentally measured non-reciprocity of mode travel times to solve the inverse problem discussed in this thesis. Once the validity of the approach is confirmed experimentally then the depth-dependent current profile in situ can be gathered covertly and continuously in support of military applications, such as AAV and MIW operations, with nothing more than the use of two hydrophones.

LIST OF REFERENCES

[1] O. A. Godin, N. A. Zabotin, and V. V. Goncharov, “Ocean tomography with acoustic daylight,” *Geophysical Research Letters*, vol. 37, no. 13, 2010. doi: 10.1029/2010gl043623.

[2] R. Snieder and K. Wapenaar, “Imaging with ambient noise,” *Physics Today*, vol. 63, no. 9, pp. 44–49, 2010. doi: 10.1063/1.3490500.

[3] K. Wapenaar, D. Draganov, R. Snieder, X. Campman and A. Verdel, “Tutorial on seismic interferometry: Part 1—Basic principles and applications,” *Geophysics*, vol. 75, no. 5, pp. 75A195-75A209, 2010. doi: 10.1190/1.3457445.

[4] K. Wapenaar, E. Slob, R. Snieder and A. Curtis, “Tutorial on seismic interferometry: Part 2—Underlying theory and new advances,” *Geophysics*, vol. 75, no. 5, pp. 75A211-75A227, 2010. doi: 10.1190/1.3463440.

[5] T. W. Tan, O. A. Godin, M. G. Brown, and N. A. Zabotin, “Characterizing the seabed in the Straits of Florida by using acoustic noise interferometry and time warping,” *The Journal of the Acoustical Society of America*, vol. 4, no. 146, pp. 2321–2334, 2019. doi: 10.1121/1.5127846.

[6] W. H. Munk, P. Worcester, and C. Wunsch, *Ocean Acoustic Tomography*. Cambridge: Cambridge University Press, 1995, pp. 47–56, 227–297.

[7] O. A. Godin, M. G. Brown, N. A. Zabotin, L. Y. Zabotina and N. J. Williams, “Passive acoustic measurement of flow velocity in the Straits of Florida,” *Geoscience Letters*, vol. 1, no. 1, 2014. doi: 10.1186/s40562-014-0016-6.

[8] M. G. Brown, O. A. Godin, X. Zang, J. S. Ball, N. A. Zabotin, L. Y. Zabotina, and N. J. WIlliams, “Ocean acoustic remote sensing using ambient noise: results from the Florida Straits,” *Geophysical Journal International*, vol. 206, no. 1, pp. 574–589, 2016. doi: 10.1093/gji/ggw170.

[9] O. A. Godin, “An effective quiescent medium for sound propagating through an inhomogeneous, moving fluid,” *The Journal of the Acoustical Society of America*, vol. 112, no. 4, pp. 1269–1275, 2002. doi: 10.1121/1.1504853.

[10] M. B. Porter, “The KRAKEN normal mode program,” [Online]. Available: http://oalib.hlsresearch.com/Modes/kraken.pdf (last viewed 04/22/2020).

[11] D. P. Winkel, M. C. Gregg, and T. B. Sanford, “Patterns of Shear and Turbulence across the Florida Current,” *Journal of Physical Oceanography*, vol. 32, no. 11, pp. 3269–3285, 2002. doi: 10.1175/1520-0485(2002)032<3269:posata>2.0.co;2.

THIS PAGE INTENTIONALLY LEFT BLANK

INITIAL DISTRIBUTION LIST

1. Defense Technical Information Center
   Ft. Belvoir, Virginia

2. Dudley Knox Library
   Naval Postgraduate School
   Monterey, California